

# Geometric Shape Effects of Surface Texture on the Generation of Hydrodynamic Pressure Between Conformal Contacting Surfaces

Haiwu Yu · Xiaolei Wang · Fei Zhou

Received: 28 February 2009 / Accepted: 4 August 2009 / Published online: 12 August 2009  
© Springer Science+Business Media, LLC 2009

**Abstract** Micro-surface texturing design is becoming an important part of surface engineering since engineering practices and analyses have indicated that surface textures may significantly affect the tribological performance of contact interfaces. Advances in the manufacturing technologies of surface finishing and micro-machining, such as laser surface texturing, photolithography, and etching, LIGA process, have made it possible to fabricate different fine structures on various engineering surfaces. Though the influence of micro-surface texturing on hydrodynamic lubrication has been widely investigated over the last decade, such an influence may be complicated and difficult to characterize with only a few statistic surface parameters. Thus, very little attention has been paid to the effects of different textural shapes and orientations on hydrodynamic lubrication, which is the main topic of this article. A theoretical model based on a single dimple was established to investigate the geometric shape and orientation effects on the hydrodynamic pressure generated between conformal contacting surfaces. Using the Successive Over Relaxation method, the average hydrodynamic pressure generated by the texture pattern with the dimples in shapes of circle, ellipse, and triangle at different orientations to the direction of sliding are obtained. The results indicate that geometric shape and orientation have obvious influences on load-carrying capacity of contacting surfaces. With the same dimple area, area ratio and dimple depth given in this research, ellipse dimples perpendicular to the sliding direction showed

the best load-carrying capacity. This result agrees with previous experimental results very well.

**Keywords** Surface texture · Geometric shapes · Load-carrying capacity · Hydrodynamic pressure

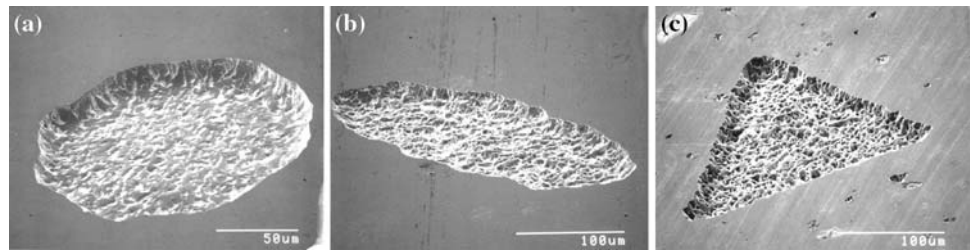
## 1 Introduction

Over the last decade, surface texturing has emerged as a viable means of enhancing tribological performance of mechanical components. As technology evolves, surface grinding, polishing, and finishing tools become available and enable the development of modern bearing surfaces. Cross-hatching of diesel cylinder liners to prevent seizure was introduced in 1940s. In recent years, modern manufacturing technologies of surface finishing and micro-machining have been developed so that it is possible to fabricate different fine structures on various engineering surfaces. As a result, various texturing techniques have been employed to improve the tribological properties of surfaces, and both theoretical and experimental studies on surface texturing for tribological applications is being carried out worldwide. For example, today, surfaces of modern magnetic storage devices are commonly textured and surface texturing is also considered as a means for overcoming adhesion and stiction in MEMS devices; Laser surface texturing (LST) is already applied successfully to mechanical seals. Both laboratory and field tests show substantial friction reduction and up to threefold increase in seal life [1]. At the same time, reactive ion etching (RIE) [2] and micro-blaster [3] are the effective texturing techniques for ceramics; micro-electrolytic etching shows great potential on the efficient texturing of metal surfaces [4] without undesirable effects on the surfaces.

---

H. Yu · X. Wang (✉) · F. Zhou  
College of Mechanical and Electrical Engineering,  
Nanjing University of Aeronautics & Astronautics,  
29# Yudao Street, Nanjing 210016, China  
e-mail: xl\_wang@nuaa.edu.cn

**Fig. 1** Surface texture of different shapes [4]. **a** circle, **b** ellipse, **c** triangle

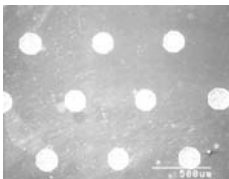
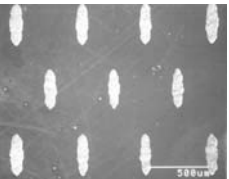
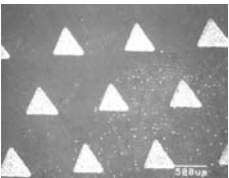


Surface texturing design is an important part of surface engineering. Significant improvement in load-carrying capacity, wear resistance, friction coefficient, etc. of tribological mechanical components can be obtained by forming reasonable surface textures on their surfaces. The mechanisms of improvement can be explained as follows: serving as a micro-hydrodynamic bearing in cases of full or mixed lubrication to generate additional hydrodynamic pressure to increase the load-carrying capacity [5]; acting as micro-reservoirs for lubricant in cases of starved lubrication conditions [6]; trapping debris to prevent severe wear on the surfaces [7]. Among these mechanisms, generating additional hydrodynamic pressure is usually considered as the most significant effect of surface texture under low-load and high-speed conditions, so that it has drawn much more focused attention [8–13]. Recently, this mechanism has begun to be studied in the elasto-hydrodynamic lubrication regime [14, 15].

In order to maximize the texture effect on the tribological performance, a great deal of fundamental research study has been carried out. For example, Halperin et al. [16] performed an experiment on laser-textured seal rings made of steel with micro-pits (pores) of various depths to demonstrate the potential of surface texturing technology. It was found that spherical segment pits with optimized size can maximize the film stiffness and the PV factor at seizure inception over untextured rings by at least 150% in oil lubrication. Wang and Kato [17] studied the anti-seizure ability of a SiC seal in water with RIE texturing. Results indicated that more than three times the critical load can be obtained with a pit diameter of 150  $\mu\text{m}$ , a pit depth of 13.3  $\mu\text{m}$ , and a pit area ratio of 5%.

Recently, several studies involving numerical simulation [10, 11, 18–21] used in the optimization of these surfaces have been published. Most researches focus on the texture of circular dimples since it is easy to be fabricated, and the

**Table 1** Geometry parameters of the patterns of dimples [4]

	Pattern and sliding directions	Depth ( $\mu\text{m}$ )	Radius ( $\mu\text{m}$ )	Area of a dimple ( $\mu\text{m}^2$ )	Pitch ( $\mu\text{m}$ )	Area ratio (%)
Circle		8	75	17671	500	7
Ellipse		8	150/37.5	17671	500	7
Triangle		8	188 (side length)	17671	500	7

parameters such as dimple density and size are studied and optimized to enhance lubrication. There are only few studies paying attention to the shape and orientation effect of the surface texture. Nanbu et al. [22] studied the effect of different texture bottom shapes on lubrication enhancement using an EHL numerical simulation. The results suggested that the texture bottom shapes involving a micro-wedge and/or a micro-step bearing tend to yield thicker films. In Ref. [4], Wang and Hsu investigated the effect of surface textural shape on the friction of lubricating steel on steel pair. Different textural shapes chosen in this article are shown in Fig. 1. The tests were conducted to check for surface-texture-orientation effects. For the non-isotropic cases, the surface features were aligned parallel and perpendicular to the direction of sliding. “Ellipse $\perp$ ” and

“Ellipse//” present the cases that sliding direction is perpendicular or parallel to the major axis of ellipse, respectively; “Triangle $\Delta\uparrow$ ” and “Triangle $\Delta\downarrow$ ” show the sliding direction that lubricant is driven toward the apex or base of the triangle, respectively. In order to obtain the effect of dimples shape and orientation, all features have the same depth, equivalent area, and same area ratio as shown in Table 1. Figures 2 and 3 show the Stribeck curves of untextured and textured specimens with the surface features oriented parallel and perpendicular, respectively, to the sliding direction. As can be seen from the figures, different geometric shapes have a different influence on friction. Ellipses placed perpendicular to the direction of sliding showed the best result of friction reduction.

In order to explain the mechanism of the effect of geometric shape and orientation reported in Ref. [4], it is required to answer whether the hydrodynamic effect is still significant in this case. Therefore, this research has developed a numerical model of a single dimple based on the steady-state Reynolds equation; the effects of different textural shape and orientation on hydrodynamic pressure were evaluated by numerical calculation.

## 2 Analytical Model

Because it is complicated and difficult to obtain analytical solution in this research, we utilize a numerical simulation method to study the effect of different textural shapes and orientations on hydrodynamic lubrication. The contacting model of two plates with relative sliding speed is displayed in Fig. 4a. The upper plate is fixed and fabricated with surface texture, and the lower plate is smooth and moving with a relative speed of  $U$  to the upper plate. The regular network of micro-dimples is textured on the upper plate with an area density  $S_p$ . An axisymmetric segment with a depth  $h_p$ , stands for each micro-dimple. Each dimple is contained within an imaginary square cell of length  $L$ . According to Ref. [18], if the area ratio of dimples is not more than 20%, the distance between neighboring pores,  $L$ , is large enough to neglect interaction between two dimples. Therefore, this imaginary square cell was used as the basic unit for calculations and the theoretical model was developed based on this unit with single dimple. Because of the difference between this single dimple model and dimples array in Ref. [4], it would introduce a certain error, but it saves computing time without altering the qualitative results.

Figure 4b shows one elliptical dimple with a long axis length of  $2a$ , short axis of  $2b$ , and a local Cartesian coordinate positioned at the center of the imaginary cell. In order to investigate the hydrodynamic pressure generated between these two surfaces, it is assumed that two plates are separated by a uniform clearance  $c$  as shown in Fig. 4a,

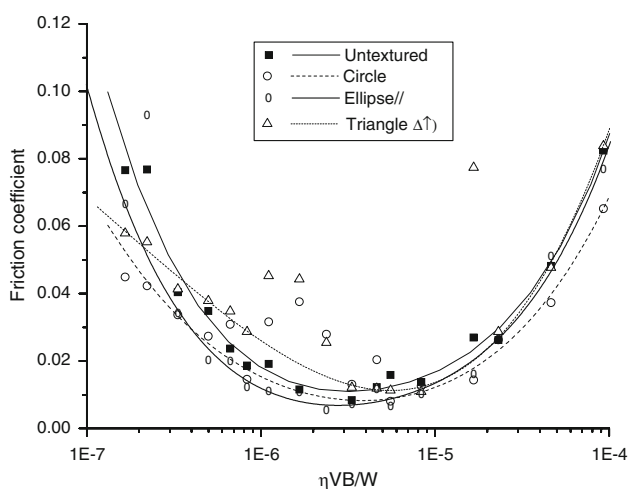


**Fig. 2** Stribeck curves of the surface features parallel to the direction of sliding ( $\eta$  is the viscosity of the lubricant,  $V$  is the sliding speed,  $B$  is the contact width, and  $W$  is the normal load) [4]

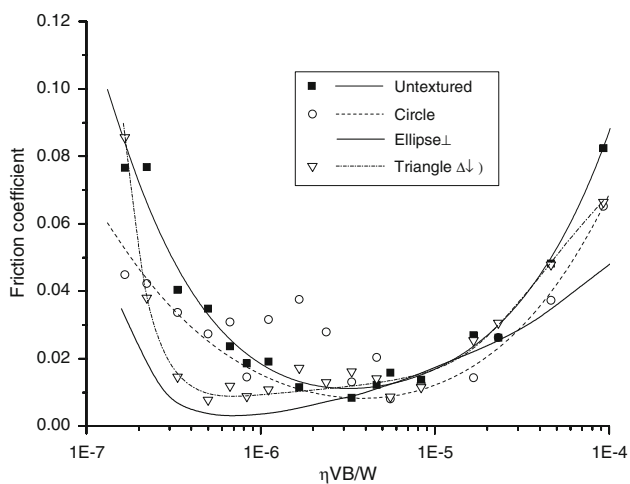
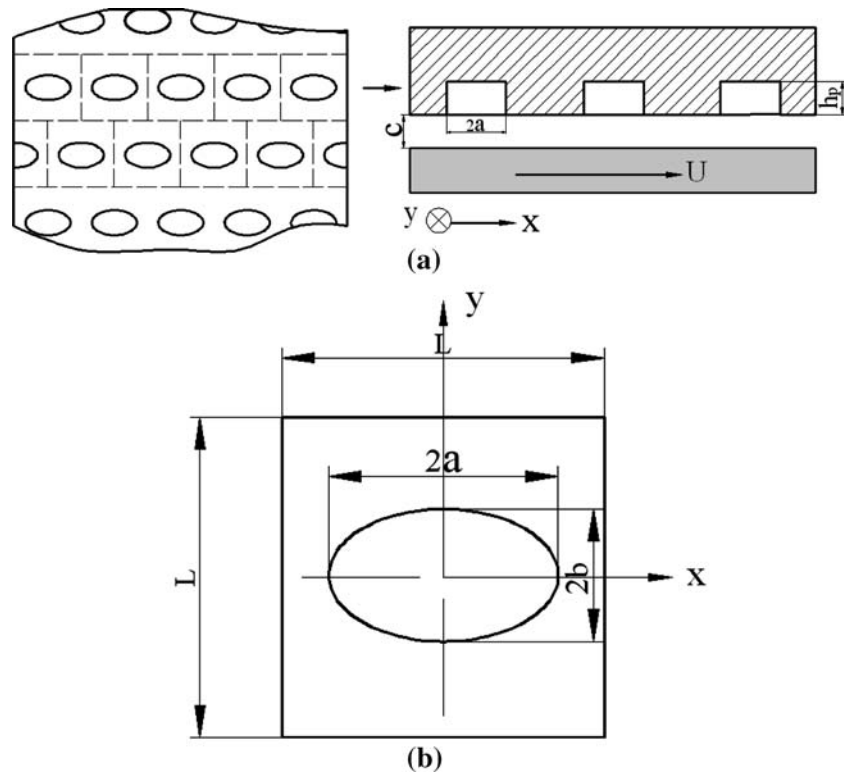


**Fig. 3** Stribeck curves of the surface features perpendicular to the direction of sliding ( $\eta$  is the viscosity of the lubricant,  $V$  is the sliding speed,  $B$  is the contact width, and  $W$  is the normal load) [4]

**Fig. 4 a** Physical model and **b** a dimple cell



the lubricant is Newtonian fluid, incompressible, and with a constant viscosity  $\eta_0$ . These assumptions are normal ways similar to that in Refs. [19–21].

The two dimensional, steady-state Reynolds equation, which relates the pressure distribution to the spacing between two disk interfaces, is given by:

$$\frac{\partial}{\partial x} \left( \frac{h^3 \partial p}{\eta \partial x} \right) + \frac{\partial}{\partial y} \left( \frac{h^3 \partial p}{\eta \partial y} \right) = 6U \frac{\partial h}{\partial x} \tag{1}$$

where  $x$  and  $y$  represent coordinates in a global Cartesian coordinate system,  $p$  is the fluid film pressure, and  $h$  is the local film thickness at a specific point. In the whole square cell,  $h$  is the summation of clearance  $c$  and the dimple depth  $h_p$  when the point is located in the dimple area, otherwise,  $h$  equal to clearance  $c$ . It can be expressed in the following form:

$$h = \begin{cases} c + h_p & (x, y) \in \text{dimple area} \\ c & \text{else} \end{cases} \tag{2}$$

To translate Eq. 1 into dimensionless form, the following dimensionless coordinates  $X$  and  $Y$ , dimensionless local film thickness  $H$  and dimensionless pressure  $P$  are defined as following:

$$X = \frac{x}{r_p}, \quad Y = \frac{y}{r_p}, \quad H = \frac{h}{c}, \quad P = \frac{p}{P_0} \tag{3}$$

where  $P_0$  is ambient pressure,  $r_p = \sqrt{ab}$ , in the case of an ellipse. The dimensionless local film thickness  $H$  as a

function of the dimensionless local coordinates  $X$  and  $Y$  for one cell is given by:

$$H = \begin{cases} 1 + \frac{h_p}{c} & (x, y) \in \text{dimple area} \\ 1 & \text{else} \end{cases} \tag{4}$$

When combining Eqs. 1 and 3, the Reynolds equation in its dimensionless form becomes:

$$\frac{\partial}{\partial X} \left( H^3 \frac{\partial P}{\partial X} \right) + \frac{\partial}{\partial Y} \left( H^3 \frac{\partial P}{\partial Y} \right) = \lambda \frac{\partial H}{\partial X} \tag{5}$$

where  $\lambda = \frac{6U\eta_0 r_p}{c^2 P_0}$

In order to get film pressure distribution between two plates, the following boundary conditions are assumed similar to Refs. [18–21]. The pressures at the boundaries of inlet ( $X = -L/2r_p$ ) and outlet ( $X = L/2r_p$ ) of lubricant are considered as ambient pressure. And the pressures at other two boundaries between adjacent dimple rows ( $Y = -L/2r_p$  and  $Y = L/2r_p$ ) are equal and changes periodic from row to row.

$$\begin{cases} P \left( X = -\frac{L}{2r_p}, Y \right) = P \left( X = \frac{L}{2r_p}, Y \right) = 1 \\ P \left( X, Y = -\frac{L}{2r_p} \right) = P \left( X, Y = \frac{L}{2r_p} \right) \\ \frac{\partial P}{\partial Y} \left( X, Y = -\frac{L}{2r_p} \right) = \frac{\partial P}{\partial Y} \left( X, Y = \frac{L}{2r_p} \right) \end{cases} \tag{6}$$

The Reynolds equation 5 was solved by a finite difference method. A grid of  $100 \times 100$  nodes/cell was chosen based on the consideration on both computing time and accuracy. The finite difference method leads to a set of

linear algebraic equations for the nodal values of the pressure which should be solved with the boundary conditions Eq. 6. The Successive Over Relaxation Method (SOR) was used to solve this linear equation set, and an over-relaxation factor of  $\varepsilon = 1.3$  was chosen to obtain a faster convergence of the pressure distribution. The converging condition is confirmed by the following equation:

$$\left| \max(P_{i,j})^k - \max(P_{i,j})^{k-1} \right| \leq 10^{-5} \quad (7)$$

where  $P_{i,j}$  is the pressure value at the point  $(i, j)$ ,  $k$  is iterative time.

### 3 Results and Discussion

In order to focus on the shape and orientation effect, the dimples used in this numerical analysis have same area, same area ratio, and same depth. And the specific texture parameters were selected to be the same as that in the experiments reported in Ref. [4], as is shown in Table 1. These specific texture parameters of the circular dimple pattern are optimized to be effective for friction reduction by the experiments. The other necessary value of parameters for calculation as follows:

- ambient pressure,  $P_0 = 0.101325$  Mpa;
- lubricant viscosity,  $\eta = 0.0228$  Pa s;
- the speed of the lower plate,  $U = 0.1, 0.2$  m/s;
- clearance,  $c = 1, 2$   $\mu\text{m}$ .

The average value  $P_{av}$  of pressure distribution  $P(x, y)$  is chosen as an index to evaluate the ability of hydrodynamic pressure generation of surface texture. Considering the Reynolds condition, on the cavitation boundary, the pressure gradient with respect to the direction normal to the boundary is zero and the pressure inside the cavitation region is retained constant close to ambient pressure. So in the course of numerical calculation, only the positive pressure was used to calculate the average value  $P_{av}$ , and the negative pressure is illustrative in the following figures.

Figure 5 shows five dimensionless hydrodynamic pressure distributions generated by different textual shapes and orientations. The flow direction of the lubricant is parallel to the  $X$  axis. As is depicted, the maximum of dimensionless pressure can be found at the right edge of the dimple. The reason for this is that additional hydrodynamic pressure was produced by the converging wedge in this area. At the left edge of the dimple, however, there is a diverging wedge resulting in a negative pressure. But the cavitation can occur in this negative pressure region according to the Reynolds boundary conditions. Consequently, there is a net additional hydrodynamic pressure.

Compared with the circular texture, Fig. 5b, d has a smaller converging wedge region and therefore a smaller hydrodynamic benefit can be found. However, Fig. 5c, e has a larger converging wedge and produce significant additional hydrodynamic pressure. So one can see that not only the textural shape can affect the additional hydrodynamic pressure but also the textural orientation. Compared with the “Ellipse//”, the “Ellipse $\perp$ ” can produce additional hydrodynamic pressure more easily. The most likely reason is that, “Ellipse $\perp$ ” results in a greater converging wedge at for the same textural parameters. “Triangle $\Delta\uparrow$ ” and “Triangle $\Delta\downarrow$ ” also displays the same trend. Of all the textural shapes and orientations, the “Ellipse $\perp$ ” shows the largest hydrodynamic pressure. Namely, the “Ellipse $\perp$ ” possesses the optimum load-carrying capacity.

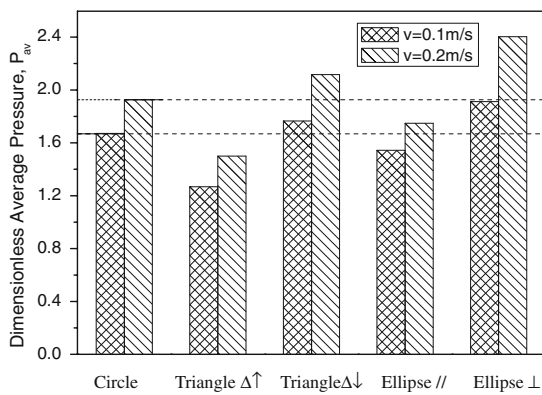
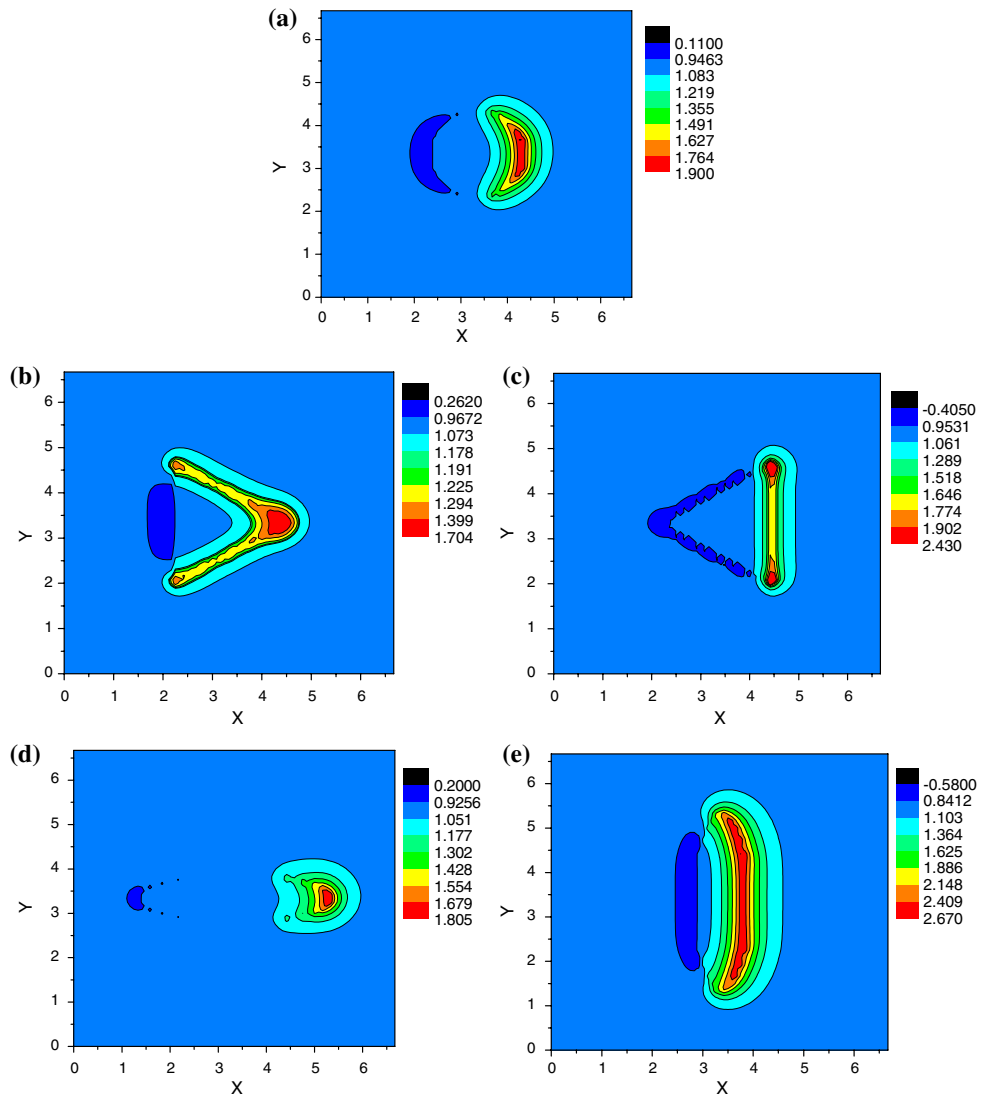
As marked in the Figs. 6 and 7, “Ellipse $\perp$ ” and “Ellipse//” present the cases that the sliding direction is perpendicular or parallel to the major axis of ellipse, respectively, “Triangle $\Delta\uparrow$ ” and “Triangle $\Delta\downarrow$ ” show the sliding directions that lubricant is driven toward the apex or base of the triangle, respectively. As mentioned above, these dimples have the same area, same area ratio, and same depth.

Figure 6 shows the effects of dimple shape and orientation on the dimensionless average pressure at a sliding speed of 0.1 and 0.2 m/s. The calculated results showed that all the texture shapes generate a hydrodynamic pressure. When the sliding speed is 0.2 m/s, the hydrodynamic pressure is higher than the pressure generated at the sliding speed of 0.1 m/s. This indicates that the effect of surface texture on hydrodynamic pressure generation is more pronounced at high speed. Most significantly, Fig. 6 shows that different texture shapes have different influences on the dimensionless average pressure even the area and depth of the dimple are the same. Compared with the circle dimple, the average dimensionless pressure  $P_{av}$  generated by “Ellipse $\perp$ ” at speed of 0.2 m/s increased by 26.3%, “Ellipse//”, however, decreased by 10.5%. Similarly, “Triangle $\Delta\downarrow$ ” increased by 10.5% when compared with the circle dimple, “Triangle $\Delta\uparrow$ ” decreased by 22%. Namely, when the texture is oriented perpendicular to the sliding direction, both “Triangle $\Delta\downarrow$ ” and “Ellipse $\perp$ ” all show dramatic improvement in the average pressure than circular texture, moreover, “Ellipse $\perp$ ” has a higher  $P_{av}$  than “Triangle $\Delta\downarrow$ ”. However, “Triangle $\Delta\uparrow$ ” and “Ellipse//” all show smaller average pressure value than the circular dimples. The same trend is depicted as well as in Fig. 7, “Ellipse $\perp$ ” shows the best result on load-carrying capacity under the clearance of 1 and 2  $\mu\text{m}$ . And the effect of texture on hydrodynamic pressure generation is more remarkable when the clearance is small.

Beside the results above, the simulation was also carried out by varying the area ratio from 3 to 30% as shown in

**Fig. 5** Dimensionless pressure distribution of different textural shapes and orientations.

**a** Circle, **b** Triangle $\Delta\uparrow$ ,  
**c** Triangle $\Delta\downarrow$ , **d** Ellipse//,  
**e** Ellipse $\perp$



**Fig. 6** Average pressure  $P_{av}$  of different textural shapes and orientations at the speed of 0.1 and 0.2 m/s

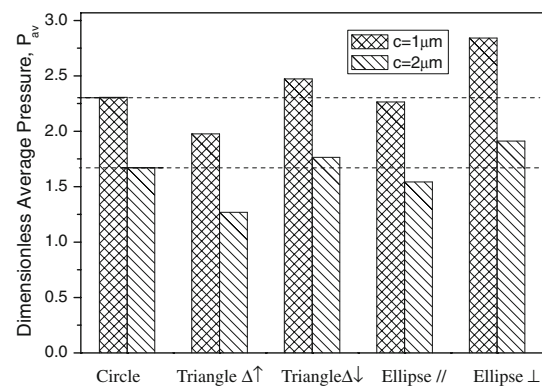


**Fig. 7** Average pressure  $P_{av}$  of different textural shapes and orientations at the clearance of 1 and 2  $\mu\text{m}$

**Fig. 8.** The dimple depth and area kept the same as shown in Table 1, and the cell length was changed to obtain different area ratio. The relative velocity is 0.1 m/s. As is

clearly seen from the figure, “Ellipse $\perp$ ” still generated maximal dimensionless average pressure  $P_{av}$  for all these five different area ratio of dimples.

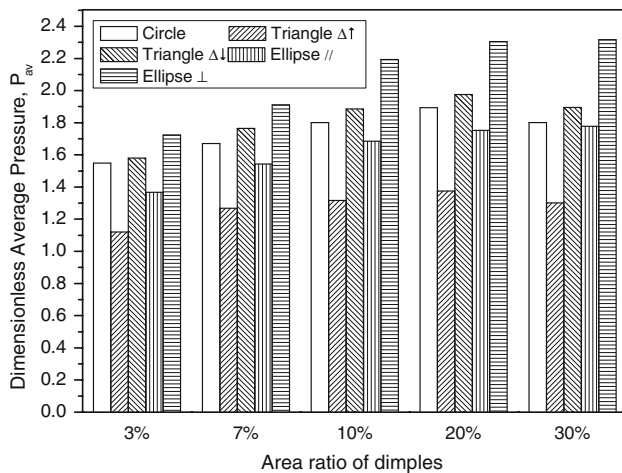


**Fig. 8** Average pressure  $P_{av}$  of different textural shapes and orientations at the different area ratio of dimple

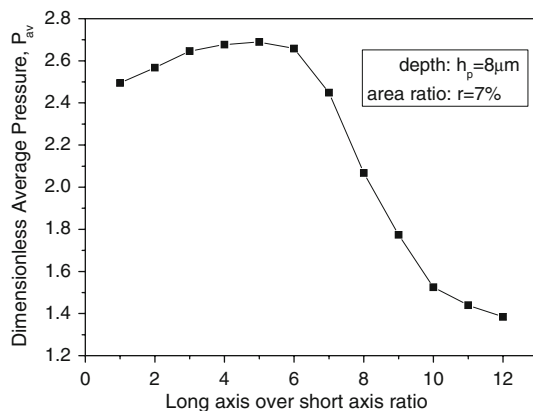


**Fig. 9** The effect of elliptical long axis over short axis ratio on dimensionless average pressure,  $P_{av}$

So we can conclude from Figs. 6, 7, and 8 that “Ellipse⊥” generated the maximum hydrodynamic pressure of all texture shapes and orientations used in this study.

According to the observations given above, it can be presumed that “Ellipse⊥” has an optimal ratio of long elliptical axis over short axis probably when the parameters such as dimple area, area ratio, and dimple depth are fixed. Figure 9 shows the results as a function of axis length ratio. It can be seen that the maximum load-carrying capacity can be obtained at the ratio range between 4 and 6. However, when the ratio is larger than 7, the load-carrying capacity is smaller than for circular dimples. Certainly, this parameter needs further study.

#### 4 Conclusion

A theoretical model was developed to investigate the effect of different textural shapes and orientations on hydrodynamic

pressure between conformal contacting surfaces. The different dimple shapes including circle, ellipse, triangle, and different orientations to the sliding direction were studied. The average dimensionless pressure was calculated and used as an index to evaluate the additional load-carrying capacity generated by the micro-dimple. It was found that the geometric shapes and orientations of dimples have an obvious influence on the load-carrying capacity. Under the condition of having the same area, same area ratio, and same dimple depth, both “Ellipse//” and “TriangleΔ↑” have smaller load-carrying capacity when compared with the circular dimple. On the contrary, “TriangleΔ↓” and “Ellipse⊥” have larger load-carrying capacity, showing a strong orientation effect. Among all the cases studied in this article, ellipses placed perpendicular to the direction of sliding showed the best result of load-carrying capacity, which increases by 26.3% over the circle dimple at the sliding speed of 0.2 m/s.

However, the theoretical model was developed just with a single dimple, the texturing parameters selected in the course of analysis are fixed, and the comparison is carried out between different geometries but with the same area, same area ratio, and same dimple depth. These fixed parameters may be different from the optimum ones corresponding to each of the individual geometries. Hence, the present conclusion is limited to that way of comparison only. Further studies need to be carried out for an array of dimples rather than just a single one, and also comparing the different geometries following optimizations of the texturing parameters for each individual geometry. Such a comparison will truly provide the ultimate best geometry for maximum load-carrying capacity.

**Acknowledgments** We would like to acknowledge the National Nature Science Foundation of China (NSFC) (No. 50675101), National High-tech R&D Program (No. 2006AA04Z321), and Science Foundation of Jiangsu province (No. BK2007529) for their financial supports.

#### References

- Etsion, I.: State of the art in laser surface texturing. *J. Tribol. Trans. ASME* **27**, 248–253 (2005)
- Wang, X.L., Adachi, K., Otsuka, K., Kato, K.: Optimization of the surface texture for silicon carbide sliding in water. *Appl. Surf. Sci.* **253**, 1282–1286 (2006)
- Wakuda, M., Yamauchi, Y., Kanzaki, S.: Effect of workpiece properties on machinability in abrasive jet machining of ceramic materials. *Precis. Eng.* **26**, 193–198 (2002)
- Wang, X.L., Hsu, S.M.: An integrated surface technology for friction control: a new paradigm effects of geometric shapes on friction. In: *The 4th China International Symposium on Tribology*. Xi’an, pp. 12–20, 8–11 Nov. 2004
- Hamilton, D.B., Walowit, J.A., Allen, C.M.: A theory of lubrication by micro-irregularities. *J. Basic Eng.* **88**, 177–185 (1966)
- Pettersson, U., Jacobson, S.: Influence of surface texture on boundary lubricated sliding contacts. *Tribol. Int.* **36**, 857–864 (2003)

7. Suh, N.P., Mosleh, M., Howard, P.S.: Control of Friction. *Wear* **175**, 151–158 (1994)
8. Ronen, A., Etsion, I., Kligerman, Y.: Friction-reducing surface-texturing in reciprocating automotive components. *Tribol. Trans.* **44**, 359–366 (2001)
9. Brizmer, V., Kligerman, Y., Etsion, I.: A laser surface textured parallel thrust bearing. *Tribol. Trans.* **46**, 397–403 (2003)
10. De Kraker, A., Van Ostayen, R.A.J., Van Beek, A., Rixen, D.J.: A multiscale method modeling surface texture effects. *J. Tribol. Trans. ASME* **129**, 221–230 (2007)
11. Brenner, G., Al-Zoubi, A., Mukinovic, M., Schwarze, H., Swo-boda, S.: Numerical simulation of surface roughness effects in laminar lubrication using the lattice-Boltzmann method. *J. Tribol. Trans. ASME* **129**, 603–610 (2007)
12. Wang, X.L., Kato, K., Adachi, K., Aizawa, K.: The effect of laser texturing of SiC surface on the critical load for the transition of water lubrication mode from hydrodynamic to mixed. *Tribol. Int.* **34**, 703–711 (2001)
13. Wang, X.L., Kato, K., Adachi, K., Aizawa, K.: Loads carrying capacity map for the surface texture design of SiC thrust bearing sliding in water. *Tribol. Int.* **36**, 189–197 (2003)
14. Chang, L., Webster, M.N., Jackson, A.: A line-contact micro-EHL model with three-dimensional surface topography. *J. Tribol.* **116**, 21–28 (1994)
15. Krupka, I., Hartl, M.: The effect of surface texturing on thin EHD lubrication films. *Tribol. Int.* **40**, 1100–1110 (2007)
16. Halperin, G., Greenberg, Y., Etsion, I.: Increasing mechanical seals life with laser-textured seal faces. In: 15th International Conference on Fluid Sealing (1997)
17. Wang, X.L., Kato, K.: Improving the anti-seizure ability of SiC seal in water with RIE texturing. *Tribol. Lett.* **14**, 275–280 (2003)
18. Etsion, I., Burstein, L.: A model for mechanical seals with regular microsurface structure. *Tribol. Trans.* **39**, 677–683 (1996)
19. Kligerman, Y., Etsion, I.: Analysis of the hydrodynamic effects in a surface textured circumferential gas seal. *Tribol. Trans.* **44**, 472–478 (2001)
20. Etsion, I., Kligerman, Y., Halperin, G.: Analytical and experimental investigation of laser-textured mechanical seal faces. *Tribol. Trans.* **42**, 511–516 (1999)
21. Raeymaekers, B., Etsion, I., Talke, F.E.: A model for magnetic tape/guide friction reduction by laser surface texturing. *Tribol. Lett.* **28**, 9–17 (2007)
22. Nanbu, T., Ren, N., Yasuda, Y., Zhu, D., Wang, Q.J.: Micro-textures in concentrated conformal-contact lubrication: Effects of texture bottom shape and surface relative motion. *Tribol. Lett.* **29**, 241–252 (2008)